Type I phosphatidylinositol 4-phosphate 5-kinase controls neutrophil polarity and directional movement

Rosa Ana Lacalle,[1] Rosa M. Peregil,[1] Juan Pablo Albar,[2] Ernesto Merino,[1] Carlos Martínez-A,[1] Isabel Mérida,[1] and Santos Mañes[1]

[1]Department of Immunology and Oncology and [2]Proteomic Facility, Centro Nacional de Biotecnología/CSIC, Darwin 3, Campus de Cantoblanco, Madrid E-28049, Spain

Directional cell movement in response to external chemical gradients requires establishment of front–rear asymmetry, which distinguishes an up-gradient protrusive leading edge, where Rac-induced F-actin polymerization takes place, and a down-gradient retractile tail (uropod in leukocytes), where RhoA-mediated actomyosin contraction occurs. The signals that govern this spatial and functional asymmetry are not entirely understood. We show that the human type I phosphatidylinositol 4-phosphate 5-kinase isoform β (PIPKIβ) has a role in organizing signaling at the cell rear. We found that PIPKIβ polarized at the uropod of neutrophil-differentiated HL60 cells. PIPKIβ localization was independent of its lipid kinase activity, but required the 83 C-terminal amino acids, which are not homologous to other PIPKI isoforms. The PIPKIβ C terminus interacted with EBP50 (4.1-ezrin-radixin-moesin (ERM)-binding phosphoprotein 50), which enabled further interactions with ERM proteins and the Rho-GDP dissociation inhibitor (RhoGDI). Knockdown of PIPKIβ with siRNA inhibited cell polarization and impaired cell directionality during dHL60 chemotaxis, suggesting a role for PIPKIβ in these processes.

Introduction

Many immune system cells detect the direction and intensity of an extracellular chemical gradient, and migrate toward the source of stimulus. This process, called chemotaxis, is essential for immune system function and homeostasis, and its deregulation is associated with chronic inflammation. Migrating cells are morphologically and functionally asymmetric, with two opposite compartments: the leading edge at the front and the uropod at the rear. Establishing and maintaining cell polarity in response to extracellular stimuli appear to be mediated by feedback loops involving phosphatidylinositol 3-kinases (PI3Ks), the Rho family of small GTPases, integrins, microtubules, and vesicular transport (Ridley et al., 2003; Charest and Firtel, 2006; Willard and Devreotes, 2006). These feedback loops are regulated in turn by the asymmetric distribution of cell membrane microdomains during migration (Gómez-Moutón et al., 2001, 2004; Mañes and Viola, 2006; Nuzzi et al., 2007).

Dynamic remodeling of actin cytoskeletal elements, which is controlled by the Rho family of GTPases, is a driving force for immune cell polarization and migration. Rac and Cdc42 GTPases are associated with leading edge protrusion and orientation of migration (Ridley et al., 2003; Willard and Devreotes, 2006); in contrast, RhoA is implicated in uropod formation (Yoshinaga-Ohara et al., 2002; Xu et al., 2003; Lee et al., 2004). RhoA activates ROCK (p160-Rho-associated coil-containing protein kinase), which phosphorylates myosin light chains (MLC) and thus increases actin filament contraction (Alblas et al., 2001; Worthylake et al., 2001). Local ATP production by mitochondria regulates myosin II phosphorylation (Campello et al., 2006).

The mechanisms by which RhoA and Rac/Cdc42 segregate to opposite poles are not well understood. In DMSO-differentiated HL60 cells (dHL60; a neutrophil-like cell line), mutual suppression of one GTPase by the other was proposed to allow Rac to predominate at the leading edge and RhoA at the uropod (Xu et al., 2003). Rac activation at the uropod has

Correspondence to Santos Mañes: smanes@cnb.uam.es

Abbreviations used in this paper: dHL60, DMSO-differentiated HL60; ERM, ezrin/radixin/moesin; EBP50, 4.1-ERM-binding phosphoprotein 50; FERM, band 4.1 protein-ezrin-radixin-moesin; *f*MLP, *N*-formyl-methionyl-leucyl-phenylalanine; KHD, kinase homology domain; MLC, myosin light chains; PBD, p21-binding domain; p-ERM, phosphorylated-ERM; PH, pleckstrin homology domain; PI3K, phosphatidylinositol 3-kinase; $PI(4,5)P_2$, phosphatidylinositol-4,5-bisphosphate; PIP_3, phosphatidylinositol 3,4,5-triphosphate; PIPKI, type I phosphatidylinositol 4-phosphate 5-kinase; PTX, pertussis toxin; RhoGDI, Rho-GDP dissociation inhibitor; ROCK, p160-Rho-associated coil-containing protein kinase.

The online version of this paper contains supplemental material.

The Journal of Cell Biology, Vol. 179, No. 7, December 31, 2007 1539–1553
http://www.jcb.org/cgi/doi/10.1083/jcb.200705044

nonetheless been reported (Gardiner et al., 2002). The signaling pathways involved in Rac/Cdc42 and RhoA activation are only partially defined. In dHL60 and Jurkat T cells, chemoattractant receptors simultaneously initiate two divergent signals, activating Rac/Cdc42 (via trimeric G_i proteins) at the leading edge and RhoA (via trimeric G_{12}/G_{13} proteins) at the uropod (Xu et al., 2003; Tan et al., 2006). Nonetheless, signaling pathways specifically triggered at the cell front may also activate RhoA at the uropod (Van Keymeulen et al., 2006; Filippi et al., 2007). In T cells, ERM proteins exercise control over RhoA activation and uropod formation (Lee et al., 2004), and can also be a downstream target of the RhoA/ROCK pathway (Yonemura et al., 2002; Yoshinaga-Ohara et al., 2002). This apparently contradictory evidence suggests a requirement for additional signaling pathways to establish front–rear cell polarity.

The lipid phosphatidylinositol 4,5-bisphosphate [$PI(4,5)P_2$] might be a key participant in the integration of the front–rear signaling. At the leading edge, $PI(4,5)P_2$ is a substrate shared by PI3K and PLC. $PI(4,5)P_2$ phosphorylation by PI3K generates phosphatidylinositol 3,4,5-triphosphate (PIP_3), a hallmark of the leading edge in polarized neutrophils (Ridley et al., 2003; Mañes et al., 2005). Antagonism between PI3K and the PIP_3 phosphatase PTEN (phosphatase and tensin homologue on chromosome 10) was proposed as a guidance system for directed migration of the amoeba *Dictyostelium* (Ridley et al., 2003), but its importance in leukocyte chemotaxis is debated (Lacalle et al., 2004; Nombela-Arrieta et al., 2004; Li et al., 2005; Van Keymeulen et al., 2006; Nishio et al., 2007). $PI(4,5)P_2$ hydrolysis by PLC generates inositol 1,4,5-triphosphate and diacylglycerol (DAG), necessary for Ca^{2+} mobilization into cells and PKC activation, respectively (Rebecchi and Pentyala, 2000). PLC activity is needed for T cell chemotaxis via a Ca^{2+}-independent/DAG-dependent mechanism (Cronshaw et al., 2006). $PI(4,5)P_2$ may also regulate cofilin location at the pseudopodia of carcinoma cells, proposed as another guidance system (Mouneimne et al., 2006). At the uropod, $PI(4,5)P_2$ is a major regulator of ERM protein activation of chemotaxing leukocytes (Yonemura et al., 2002; Fievet et al., 2004), and directly regulates many actin-binding and actin-remodeling proteins, including Rho GTPases (Caroni, 2001; Ling et al., 2006). Given the high steady-state level of $PI(4,5)P_2$ and the broad range of its potential targets, functional compartmentalization of $PI(4,5)P_2$ inside the cell may be crucial during chemotaxis.

Although $PI(4,5)P_2$ can be synthesized from PI(5)P (Rameh et al., 1997), the main biosynthetic pathway is regulated by the so-called type I phosphatidylinositol-phosphate kinases (PIPKIs), which use PI(4)P as substrate and thus function as PI(4)P-5 kinases (Ishihara et al., 1998). There are three PIPKI isoforms (α, β, and γ); human PIPKIα is equivalent to the mouse PIPKIβ isoform and vice versa (to avoid confusion, we will use human nomenclature in this manuscript). There are also at least two PIPKIγ isoforms ($PIPKI\gamma^{635}$ and $PIPKI\gamma^{661}$), generated by alternative splicing. In fibroblasts, the three PIPKI isoforms have distinct subcellular locations (Ling et al., 2006).

Here, we found that the human PIPKIβ isoform localizes to the uropod of polarized dHL60 cells; this polarized distribution requires the PIPKIβ C-terminal domain. At the uropod, PIPKIβ may serve as a scaffold for interaction among several proteins including, but not limited to, EBP50, ERM, and RhoGDI. PIPKIβ knockdown impaired cell polarity and directionality during chemotaxis. We thus propose PIPKIβ as a new element involved in a positive feedback loop that regulates directional leukocyte motility by organizing specific signaling pathways at the cell posterior.

Results

Human PIPKIβ localizes to the uropod of polarized dHL60 cells

To study $PI(4,5)P_2$ compartmentalization in leukocyte chemotaxis, we used real-time videomicroscopy to analyze localization of the mouse orthologues for three GFP-tagged PIPKI isoforms (PIPKIα, PIPKIβ, and $PIPKI\gamma^{635}$) in dHL60 cell chemotaxis toward the neutrophil chemoattractant *N*-formyl-methionyl-leucyl-phenylalanine (*f*MLP). We found that as the cells polarized, GFP-PIPKIβ accumulated almost exclusively at the sides and back of moving cells (Fig. 1 A; Video 1, available at http://www.jcb.org/cgi/content/full/jcb.200705044/DC1). In contrast, GFP-PIPKIα and GFP-$PIPKI\gamma^{635}$ homogeneously stained the cytosol and/or membrane, with no specific cell pole dominance during chemotaxis (Fig. 1 A; Videos 2 and 3). HA-tagged PIPKIβ also localized at the uropod of *f*MLP-stimulated dHL60 cells, indicating that uropod localization of this PIPK isoform was not the consequence of GFP fusion (Fig. S1 A, available at http://www.jcb.org/cgi/content/full/jcb.200705044/DC1). Immunofluorescence analysis of endogenous PIPKI isoforms in *f*MLP-stimulated dHL60 cells suggested PIPKIβ accumulation at the uropod (Fig. 1 B; Fig. S1 B). Finally, GFP-tagged PIPKIβ was confined at the uropod of Jurkat T cells polarized by CXCL12 stimulation, indicating that PIPKIβ localization at the cell rear is found in different cell types (Fig. S1 C).

PIPKIβ is required for dHL60 cell polarity and chemotaxis

To address the relevance of PIPKIβ in chemotaxis, we transfected dHL60 cells with mismatched or PIPKIβ-specific siRNA. Two different PIPKIβ-siRNAs reduced mRNA levels specifically for PIPKIβ, but did not affect the other PIPKI isoforms (Fig. 2 A); moreover, these PIPKIβ siRNAs reduced PIPKIβ protein levels (Fig. 2 B). Targeting of endogenous PIPKIβ significantly reduced dHL60 cell polarization, as determined by the concurrent loss of F-actin accumulation at the leading edge and of phosphorylated-ERM (p-ERM) at the uropod (Fig. 2 C). Moreover, PIPKIβ-specific, but not mismatched siRNA, reduced dHL60 chemotaxis toward *f*MLP in a transwell assay (Fig. 2 D). To further analyze the role of PIPKIβ in chemotaxis, we performed time-lapse chemotactic assays of control and PIPKIβ-specific siRNA-transfected dHL60 cells. PIPKIβ-specific siRNA significantly impaired persistence during migration (0.85 ± 0.02 vs. 0.69 ± 0.03, for control and PIPKIβ siRNA-transfected cells, respectively; $P < 0.001$, two-tailed *t* test), but did not affect cell speed (7.84 ± 0.34 μm/min for control, 8.17 ± 0.6 μm/min for PIPKIβ-siRNA, $P = 0.63$, two-tailed *t* test;

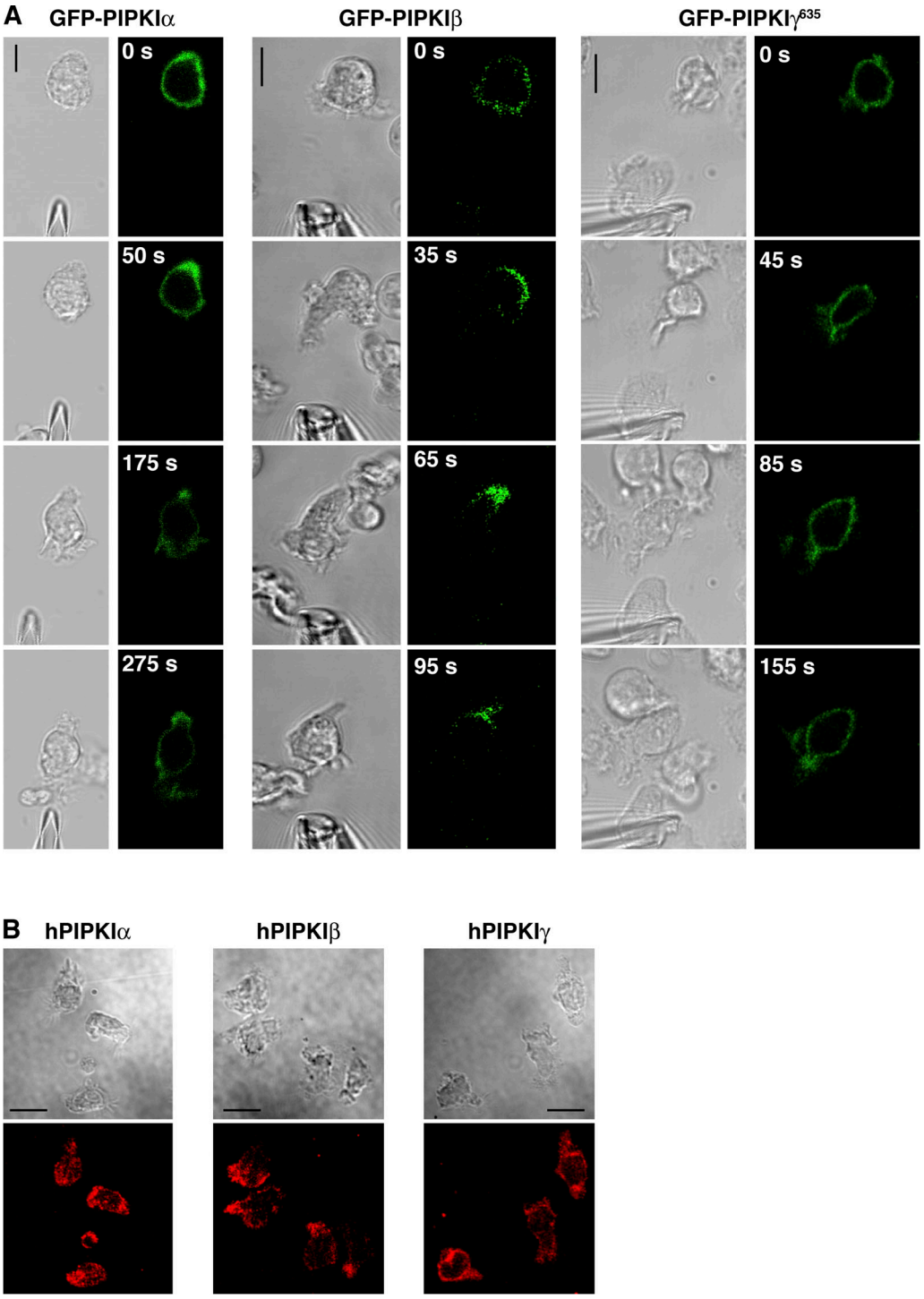

Figure 1. **Human PIPKIβ polarizes to the uropod during dHL60 cell chemotaxis.** (A) Time-lapse Nomarski and fluorescent images of dHL60 cells expressing GFP-tagged PIPKIα, PIPKIβ, and PIPKIγ^{635} isoforms migrating toward an *f*MLP-loaded micropipette. Time in seconds from the first frame (0 s). (B) Immunofluorescence analysis of endogenous PIPKI isoforms in uniformly stimulated dHL60 cells. Bar, 10 μm. Results are representative of at least 20 cells recorded in each of three independent experiments.

Fig. 2 E). The mean translocation rate over a 7-min period was also higher in PIPKIβ siRNA (11.26 ± 0.41 μm/min) than in control siRNA (9.89 ± 0.49 μm/min) transfected cells ($P = 0.07$, two-tailed *t* test). These results suggest a role for endogenously expressed PIPKIβ in the chemoattractant-elicited leukocyte cell polarity program.

Signaling pathways involved in uropod accumulation of PIPKIβ

Chemoattractant stimulation in leukocytes appears to generate two opposing signals, mediated by different trimeric G proteins; pertussis toxin (PTX)-sensitive G_i proteins activate leading edge signaling pathways, and PTX-insensitive G_{12}/G_{13} elicit the

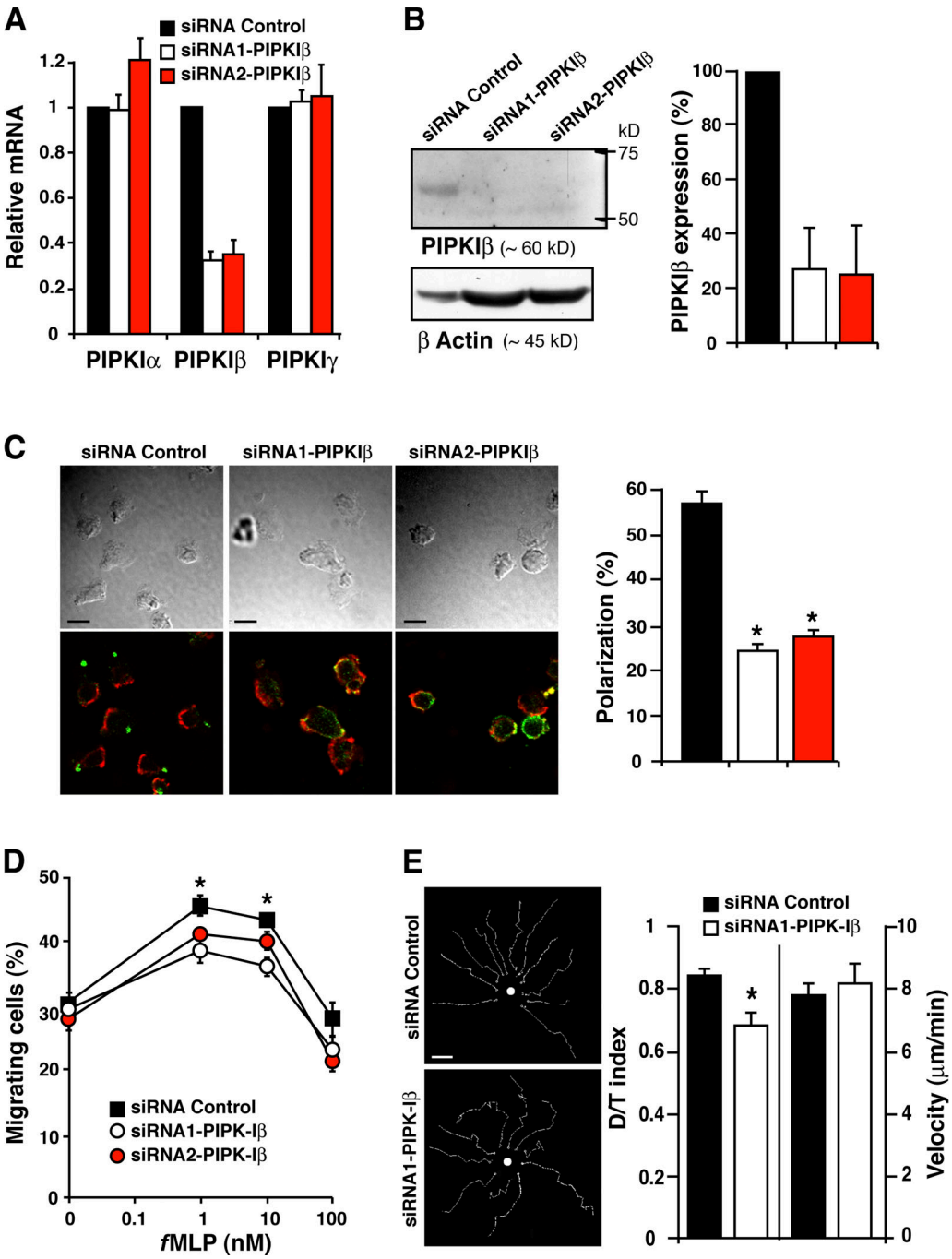

Figure 2. **PIPKIβ knockdown inhibits dHL60 cell polarization and chemotaxis.** (A) PIPKIβ knockdown in dHL60 cells 48 h after transfection with 50 nM control or PIPKIβ-specific siRNA, as determined by quantitative RT-PCR (see Materials and methods). The results are normalized to the relative PIPKIβ mRNA levels in cells transfected with control siRNA (representative of five experiments). (B) Crude lysates (80 μg/lane) from cells as in A were analyzed by immunoblot with anti-PIPKIβ and anti-actin antibodies. The graph represents mean ± SEM of densitometry values for the PIPKIβ band from three independent experiments, taking the band in siRNA control cells as 100%. (C) Cell polarity depends on PIPKIβ. Uniformly stimulated dHL60 cells transfected with control or two PIPKIβ-specific siRNA were stained with phalloidin (red) and phospho-ERM proteins (green) as leading edge and uropod markers, respectively. Only cells showing clear segregation of phalloidin and phospho-ERM proteins were scored as polarized. Data are mean ± SEM of the percentage of polarized cells from three independent experiments. Representative fields for each condition are shown (left panels). Bar, 10 μm. (D) Cell chemotaxis depends on PIPKIβ. Chemotaxis was analyzed for Cy3-labeled control or PIPKIβ-specific siRNA-transfected dHL60 cells in transwell assays (see Materials and methods). Data are mean ± SEM (expressed as percentage) of cells migrating toward *f*MLP in three independent experiments. (*, $P < 0.01$; two-tailed *t*-test). (E) Representative examples of migration tracks of control or PIPKIβ-specific siRNA-transfected cells chemotaxing toward *f*MLP. In these and subsequent composite migration figures, randomly selected individual migration tracks were copied and combined into a single figure. The white dot represents the *f*MLP-loaded pipette tip; bar, 10 μm. Right panels show quantification of the persistence of migratory directionality and velocity of control or PIPKIβ siRNA-transfected cells. D/T ratios represent the ratio of the direct distance from start to end point [D] divided by total track distance [T]. Velocity was calculated as total distance divided by time (μm/min). Data were pooled from three independent experiments; error bars indicate SEM based on $n = 22–25$ cells (*, $P < 0.001$; two-tailed *t* test).

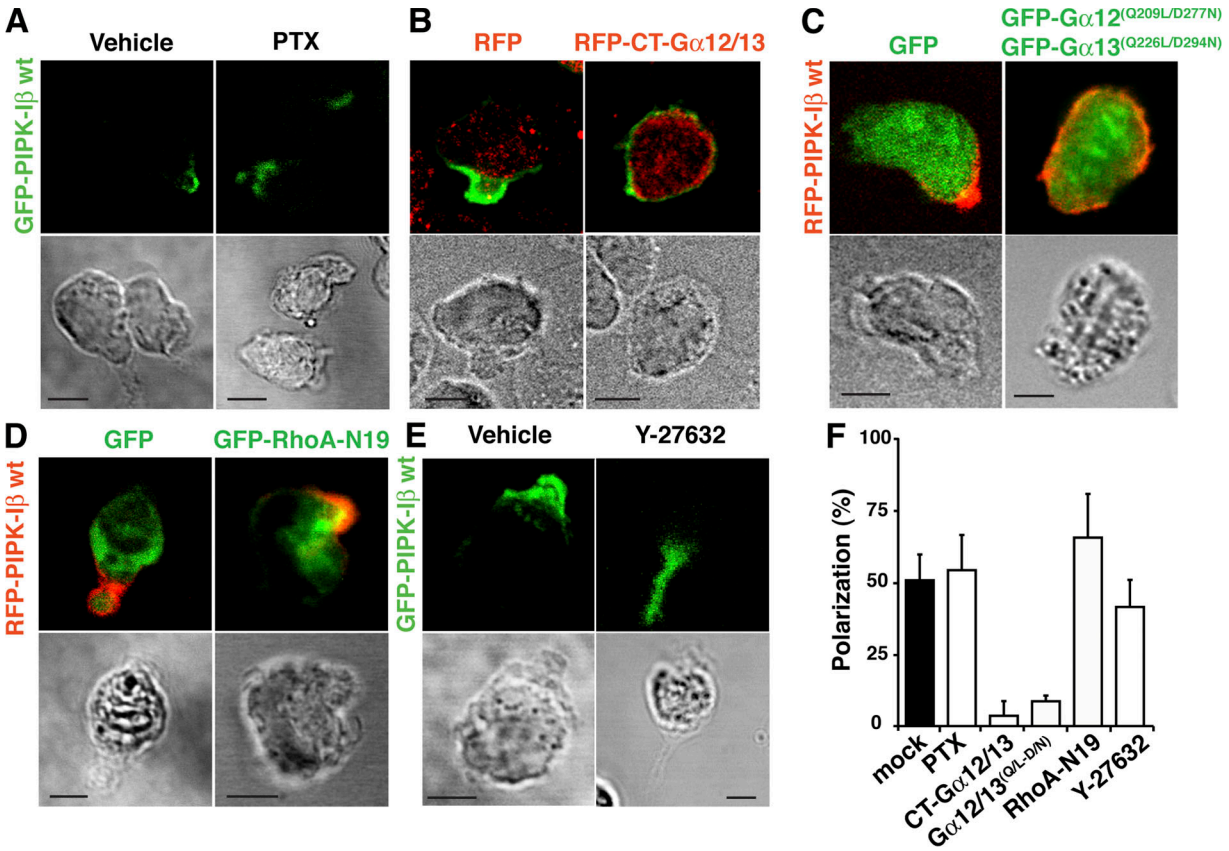

Figure 3. **Signaling pathways involved in PIPKIβ polarization.** Polarization of GFP- or RFP-tagged PIPKIβ was analyzed in *f*MLP-stimulated dHL60 cells after treatment with PTX (A), overexpression of dominant-negative $G\alpha_{12}$ and $G\alpha_{13}$ mutants (B), overexpression of the catalytically inactive $G\alpha_{12}^{(Q209L/D277N)}$ and $G\alpha_{13}^{(Q226L/D294N)}$ mutants (C), dominant-negative GFP-RhoAN19 mutant (D), or after treatment with ROCK inhibitor Y-27632 (E). Mock-transfected or vehicle-treated cells were analyzed in parallel. Representative cells in each experimental condition are shown; bar, 10 μm. (F) Quantification of the effect on PIPKIβ polarization of the inhibitors or mutants tested. Data are mean ± SEM from three independent experiments; at least 30 cells were recorded in each experiment for each condition.

signals that shape the uropod (Xu et al., 2003; Tan et al., 2006). PTX treatment of dHL60 cells did not prevent *f*MLP-induced PIPKIβ accumulation at the uropod (Fig. 3 A; quantification in Fig. 3 F). Overexpression of the C terminus of $G\alpha_{12}$ and $G\alpha_{13}$, or of the catalytically inactive $G\alpha_{12}^{(Q209L/D277N)}$ and $G\alpha_{13}^{(Q226L/D294N)}$ mutants, prevented PIPKIβ polarization (Fig. 3, B and C).

We analyzed PIPKIβ polarization in dHL60 cells expressing a dominant-negative RhoA mutant (RhoAN19). Although RhoAN19 overexpression altered the dHL60 cell phenotype, PIPKIβ concentration at the uropod persisted in a large proportion of cells (Fig. 3 D). ROCK is a major RhoA target, and controls actomyosin contraction by regulating the phosphorylation state of MLC (Kimura et al., 1996). Cell treatment with the ROCK inhibitor Y-27632 resulted in cells with extended uropods, probably due to the inability of the cell to retract the rear; indeed, Y-27632 treatment greatly reduced dHL60 cell migration (unpublished data). PIPKIβ was localized diffusely in these long uropods, but was excluded from the leading edge (Fig. 3 E), indicating that ROCK inhibition did not prevent PIPKIβ polarization. These results suggest that PIPKIβ polarization is independent of RhoA signaling.

The PIPKIβ C terminus acts as a uropod-targeting sequence

We studied the molecular determinants for specific PIPKIβ recruitment to the uropod. PIPKI has a conserved kinase homology domain (KHD) and sequence-divergent N and C termini; we thus performed mutagenesis analysis that affected each of these regions (Fig. 4 A). Lipid kinase activity appeared not to be required for PIPKIβ-specific location, as the kinase-dead $PIPKI\beta^{K138A}$ mutant (Itoh et al., 2000) concentrated at the uropod of polarized cells, as did PIPKIβwt (Fig. 4, B and C; Fig. S1 D). Many $PIPKI\beta^{K138A}$-expressing cells nonetheless had longer tails than PIPKIβwt-expressing cells (Video 4, available at http://www.jcb.org/cgi/content/full/jcb.200705044/DC1). Consistent with this impairment in tail retraction, cell speed was reduced in $PIPKI\beta^{K138A}$-expressing dHL60 cells compared with mock- or PIPKIβwt-expressing cells (7.0 ± 0.6 μm/min for PIPKIβwt vs. 3.9 ± 0.3 μm/min for the $PIPKI\beta^{K138A}$ mutant; Fig. 4 J). $PIPKI\beta^{K138A}$-expressing cells also showed a significant reduction in directionality compared with PIPKIβwt-expressing cells (Fig. 4, I and J).

Within the KHD, the activation loop (PIPKIβ amino acids 355–376) confers substrate specificity, whereas K^{397} and K^{398} are important for membrane anchoring (Arioka et al., 2004). In PIPKIγ, the KHD N-terminal portion is also required for membrane association (Arioka et al., 2004), suggesting that the KHD is necessary and sufficient for plasma membrane localization. Our results confirmed these observations, as GFP-tagged PIPKIβΔ34 (Fig. 4 D) and PIPKIβΔ395 (Fig. 4 E) deletion mutants localized to cytosol. These mutants were also homogeneously distributed in

polarized cells, indicating that plasma membrane association is a major determinant for PIPKIβ polarization at the uropod.

The PIPKIβΔ456 mutant, which retains KHD but lacks the last 83 amino acids (83aa-tail), retained membrane association but was homogeneously distributed in *f*MLP-stimulated cells (Fig. 4 F). To further confirm the role of this 83aa-tail in uropod targeting, we produced a chimeric protein by fusing the 83aa-tail of PIPKIβ to a C terminus–deleted PIPKIγ mutant (PIPKIγ$^{1\text{-}502}$). PIPKIγ$^{1–502}$ stained the cell periphery evenly (Fig. 4 G; Video 5, available at http://www.jcb.org/cgi/content/full/jcb.200705044/DC1); introduction of the 83aa-tail from the β isoform into this mutant (PIPKIγ$^{1–502}$β$^{455–539}$) was sufficient to redirect this chimera to the uropod (Fig. 4 H; Video 6), indicating the relevance of the PIPKIβ C terminus for uropod polarization. When expressed alone in dHL60 cells, the 83aa-tail localized in the perinuclear region (unpublished data), supporting the idea that PIPKIβ localization at the uropod requires kinase binding to the plasma membrane.

We also observed dose-dependent inhibition of chemoattractant-induced cell asymmetry by PIPKIβΔ456 overexpression. Time-lapse experiments indicated that PIPKIβΔ456-expressing cells were unable to chemotax toward *f*MLP, showing a severe reduction in cell directionality and speed (Fig. 4, I and J). Introduction of the 83aa-tail in the chimera PIPKIγ$^{1–502}$β$^{455–539}$ restored cell velocity (6.1 ± 0.5 μm/min), although directionality was reduced compared with PIPKIβwt-expressing cells (0.83 for PIPKIβwt vs. 0.75 for PIPKIγ$^{1–502}$β$^{455–539}$; Fig. 4 J; borderline significance). This small difference in directional persistence in PIPKIγ$^{1–502}$β$^{455–539}$-expressing cells suggests nontotally overlapping functions for other domains of PIPKIβ and PIPKIγ isoforms in cell chemotaxis.

Overexpression of the PIPKIβΔ456 mutant prevents cell orientation toward a gradient

To further study the loss of polarity induced by PIPKIβΔ456 overexpression, we analyzed the asymmetry of early *f*MLP-induced signals. The AKT-PH domain (AKT-PH-GFP) is recruited persistently at the up-gradient edge in dHL60 cells (Gómez-Moutón et al., 2004), and this pattern was not changed by PIPKIβwt overexpression (Fig. 5 A; Video 7, available at http://www.jcb.org/cgi/content/full/jcb.200705044/DC1). In PIPKIβΔ456-overexpressing cells, AKT-PH-GFP was recruited simultaneously to pseudopods formed on the cell down- and up-gradient sides (Fig. 5 B; Video 8). We also analyzed the dynamics of the GFP-tagged Pak-1 binding domain (PBD-GFP) to monitor active Rac, a pathway involved in leading edge formation. PBD-GFP cycled between the cytosol and the membrane exclusively at the leading edge of PIPKIβwt-expressing cells during chemotaxis (Fig. 5 C; Video 9). In PIPKIβΔ456 cells, however, PBD-GFP was recruited very transiently to pseudopods that formed around the cell perimeter (Fig. 5 D; Video 10). Together, these results indicate that PIPKIβΔ456 prevents morphological and functional polarization of chemoattractant-stimulated dHL60 cells, even though these cells express endogenous PIPKIβ.

PIPKIβΔ456 might induce this dominant-negative effect on cell polarity by deregulating PI(4,5)P_2 levels. PIPKIβΔ456 retains intact KHD and the activation loop, and therefore this mutant might retain the ability to produce PI(4,5)P_2. To address this point, we performed an in vitro kinase assay using HA-PIPKIβwt and HA-PIPKIβΔ456 immunoprecipitated from HEK-293 cells before or after stimulation with the chemoattractant CXCL12. Both HA-PIPKIβwt and HA-PIPKIβΔ456 showed basal kinase activity in unstimulated cells, which increased after chemoattractant stimulation (Fig. 5 E). Generation of PI(4,5)P_2 was not observed in immunoprecipitates of the kinase-dead HA-PIPKIβ^{K138A} or HA-PIPKIβΔ456^{K138A} mutants, indicating kinase assay specificity (Fig. 5 E). These results thus suggest that chemoattractants stimulate PIPKIβ lipid kinase activity. Chemoattractant stimulation nonetheless did not increase total PI(4,5)P_2 levels in PIPKIβwt- or HA-PIPKIβΔ456-expressing cells (Fig. S2 A, available at http://www.jcb.org/cgi/content/full/jcb.200705044/DC1); furthermore, total PI(4,5)P_2 levels were not increased by PIPKIβwt or HA-PIPKIβΔ456 overexpression, compared with mock-transfected cells.

We thus analyzed local changes in PI(4,5)P_2 during PIPKIβwt- and PIPKIβΔ456-expressing dHL60 cell chemotaxis using the pleckstrin homology (PH) domain of PLCδ tagged with GFP (GFP-PH-PLCδ). Overexpression of GFP-PH-PLCδ drastically inhibited chemotaxis in these cells (unpublished data), however, compromising data interpretation. A considerable proportion of GFP-PH-PLCδ–expressing dHL60 still polarized after homogeneous stimulation with *f*MLP. In polarized mock and RFP-PIPKIβwt-expressing cells, GFP-PH-PLCδ accumulated at the leading edge and the uropod (Fig. S2, B and C). In contrast, PI(4,5)P_2 co-redistributed with RFP-PIPKIβΔ456 in random patches in the periphery of PIPKIβΔ456-expressing cells (Fig. S2 D).

Because chemoattractants stimulate PIPKIβΔ456-mediated PI(4,5)P_2 production, PIPKIβΔ456 might prevent dHL60 cell polarization by "delocalizing" the source of PI(4,5)P_2; elevated PI(4,5)P_2 levels might in turn generate PIP_3 at inappropriate cell sites. A kinase-dead version of PIPKIβΔ456 (PIPKIβΔ456^{K138A}) nonetheless inhibited *f*MLP-induced dHL60 cell polarization as efficiently as the kinase-active PIPKIβΔ456 (Fig. 5 F); moreover, *f*MLP-induced AKT phosphorylation, an indirect readout of PIP_3 levels, was comparable in cells expressing the kinase-active or kinase-dead mutants (Fig. S2 E). These results indicate that the dominant-negative effects of PIPKIβΔ456 on cell polarity are independent of its lipid kinase activity. PIPKIβwt overexpression also restored *f*MLP-induced cell polarity in PIPKIβΔ456-expressing dHL60 cells (Fig. 5 G), suggesting that through a region distinct from the C terminus, PIPKIβ binds to other protein(s) with an important role in cell polarity.

Overexpression of the PIPKIβΔ456 mutant inhibits RhoA activation at the uropod

We found that PIPKIβΔ456 overexpression resulted in homogeneous, largely cytosolic distribution of RhoA after uniform *f*MLP stimulation, which contrasted with the uropod RhoA distribution in PIPKIβwt-expressing cells (Fig. 6 A). Stimulation of untransfected dHL60 or HEK-293 cells with *f*MLP or the chemokine CXCL12, respectively, induced a transient increase in RhoA activity after 30–60 s (Fig. S3A, available at http://www.jcb.org/cgi/content/full/jcb.200705044/DC1).

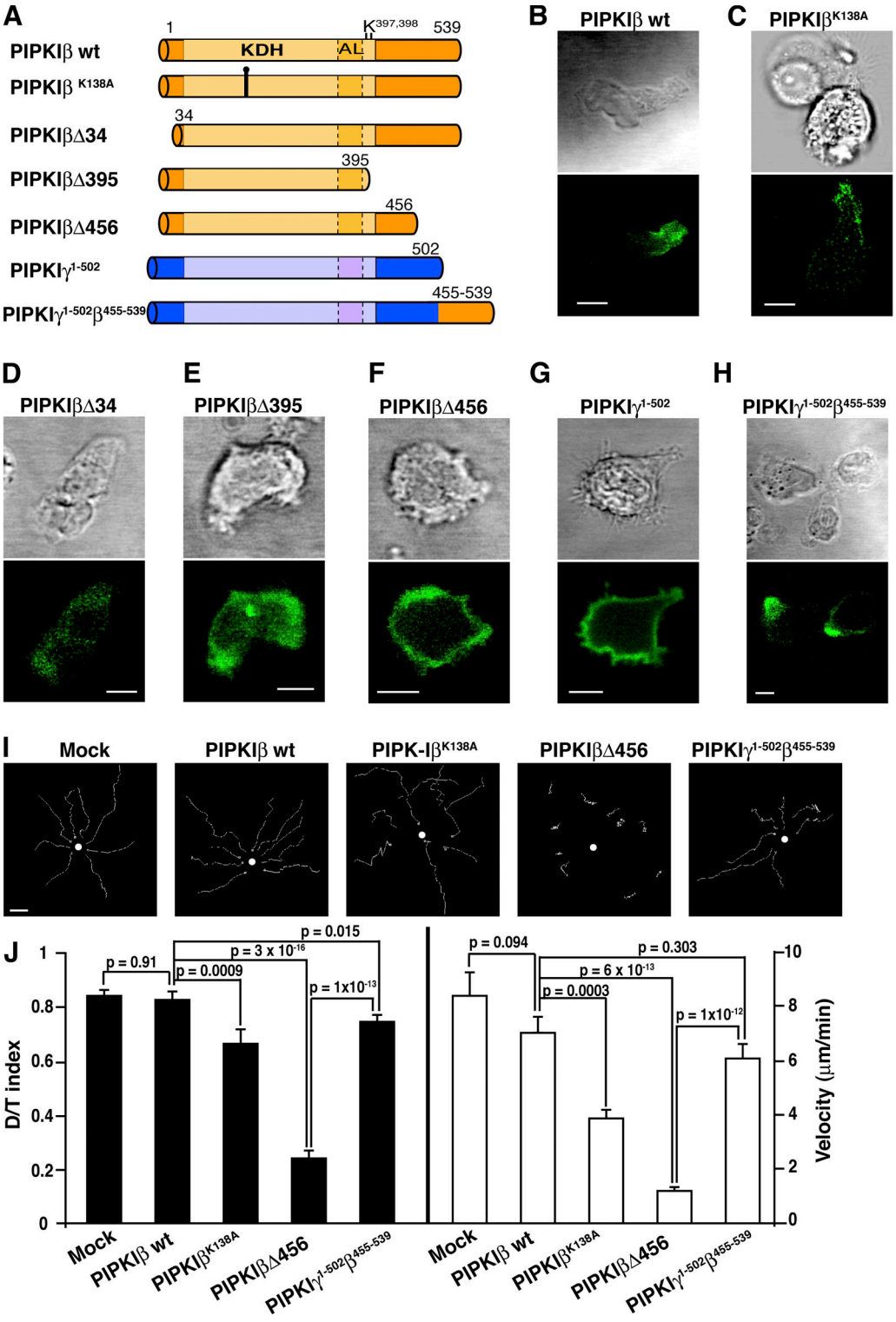

Figure 4. **Polarization of PIPKIβ to the cell uropod requires the C terminus.** (A) Scheme of the PIPKIβ mutants and chimeras used. The KHD is shown in pastel colors; the activation loop (AL) is delimited by dashed lines. The K^{138A} mutation is indicated by a solid line. (B–H) subcellular distribution of the different GFP-tagged mutants in polarized dHL60 cells after uniform stimulation with *f*MLP. Cells are representative of at least 20 cells recorded in three independent experiments; bar, 10 μm. (I) Composite collection of representative tracks for *f*MLP-induced migration of dHL60 cells expressing the indicated PIPKIβ mutants; bar, 10 μm. (J) Quantification of persistence of migratory directionality (D/T) and velocity of the transfected cells. Data (mean ± SEM) were obtained from video time-lapse microscopy of a total of 18–25 cells. Probability was calculated by two-tailed *t*-test and is indicated for the corresponding mutants. The mean translocation rates (± SEM), calculated as total cell migration over 2–5-min periods (or 2–8 min for the $PIPKIβ^{K138A}$ mutant), were 16.1 ± 0.75, 13.57 ± 0.66, 6.11 ± 0.62, 4.47 ± 0.27, and 11.08 ± 0.57 μm/min for mock-, PIPKIβwt-, $PIPKIβ^{K138A}$-, PIPKIβΔ456-, and $PIPKIγ^{1–502}β^{455–539}$-expressing cells, respectively.

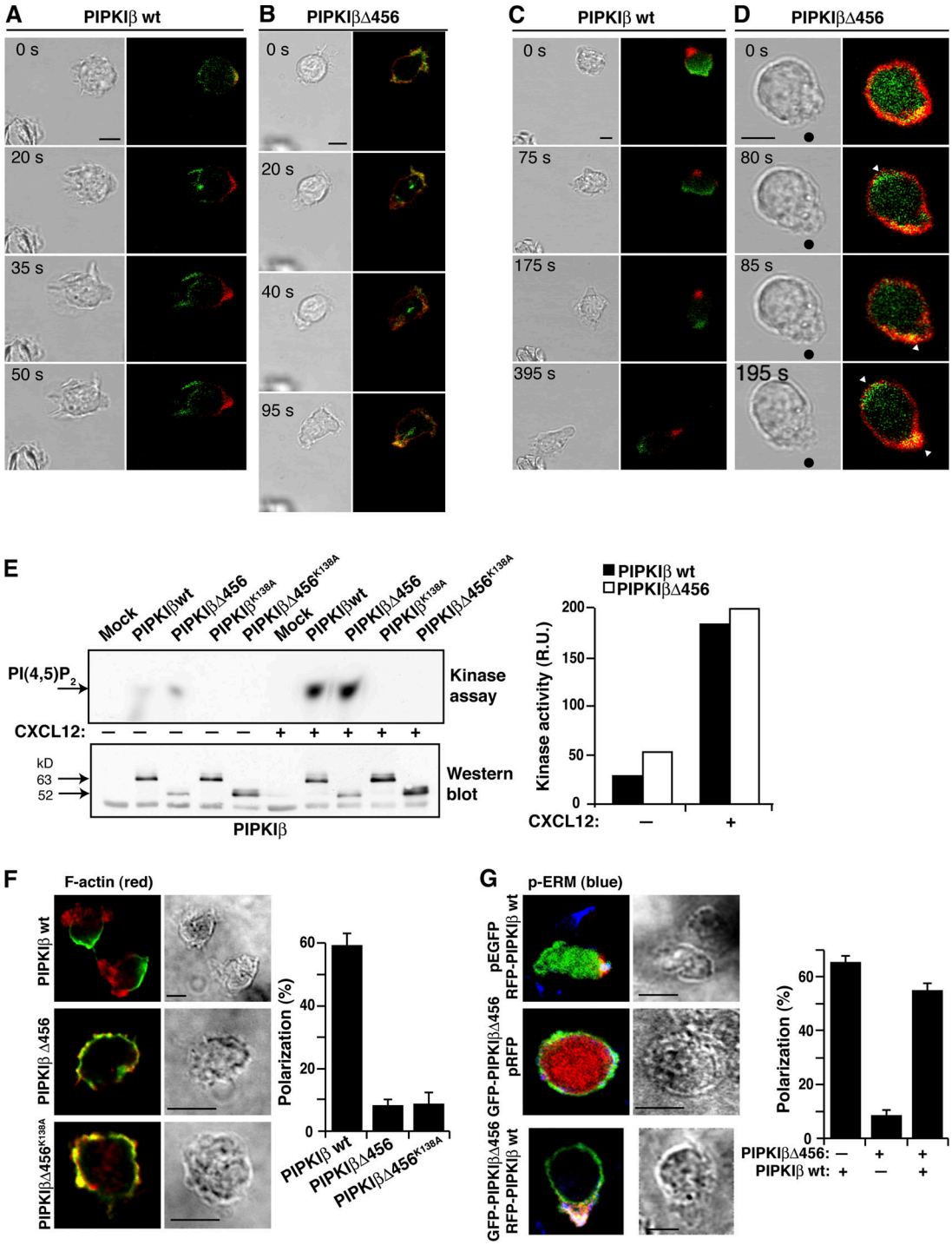

Figure 5. **Overexpression of PIPKIβΔ456 prevents dHL60 cell polarity.** (A–D) PI3K and Rac activation were analyzed by time-lapse video microscopy of RFP-PIPKIβwt- and RFP-PIPKIβΔ456-expressing dHL60 cells, using the AKT-PH-GFP (A and B) and the PBD-GFP (C and D) domains as probes for PI3K and Rac, respectively. Time-lapse images for Nomarski and red-green channel merge are shown. In D, micropipette location is indicated by a black dot; arrowheads indicate areas of the membrane recruiting the PBD-GFP probe. The cells shown are representative of at least 30 recorded in three independent experiments. (E) Chemoattractants stimulate PIPKIβ- and PIPKIβΔ456-induced PI(4,5)P_2 production. HA-tagged PIPKIβ constructs as indicated were immunoprecipitated from starved or CXCL12-stimulated HEK-293 cells; kinase activity was analyzed in an in vitro kinase assay using PI(4)P as substrate. The same cell extracts were analyzed by immunoblot to determine the expression of each PIPKIβ construct (bottom panel). The right panel shows densitometry values for the PI(4,5)P_2 band. One representative experiment of two is shown. (F) PIPKIβΔ456 kinase activity is dispensable for prevention of cell polarity. PIPKIβ-, PIPKIβΔ456-, or kinase-dead PIPKIβΔ456^{K138A}-expressing dHL60 cells were stimulated with *f*MLP and stained with phalloidin (red) to detect F-actin. Quantification of polarized cells, determined as phalloidin staining at the leading edge, is shown (right panel). (G) PIPKIβ overexpression restores cell polarity in PIPKIβΔ456-expressing cells. dHL60 cells were transfected with the indicated plasmids mixtures (pRFP-PIPKIβ and pEGFP; pGFP-PIPKIβΔ456 and pRFP; pRFP-PIPKIβ and pGFP-PIPKIβΔ456) at a 1:1 ratio. After stimulation, cells were stained for phospho-ERM (blue). Single-color images are provided as supplemental material (available at http://www.jcb.org/cgi/content/full/jcb.200705044/DC1). Only cells showing phospho-ERM staining at the uropod were scored as polarized (right panel). The cells shown (A–D, F, and G) are representative of at least 30 recorded in three independent experiments. Error bars indicate SEM. Bar, 10 μm.

This pattern was not altered in mock- or PIPKIβ-expressing cells, but PIPKIβΔ456 overexpression reduced chemoattractant-induced RhoA activation (Fig. 6 B). siRNA-induced reduction of endogenous PIPKIβ also diminished *f*MLP-induced RhoA activation in dHL60 cells (Fig. 6 C), suggesting PIPKIβ involvement in RhoA activation.

We next analyzed the phosphorylation of MLC (pS^{19}-MLC), a target of the RhoA-ROCK pathway, in *f*MLP-stimulated cells. We found an acute reduction in pS^{19}-MLC in PIPKIβΔ456-expressing cells compared with PIPKIβwt-expressing cells (Fig. 6 D); pS^{19}-MLC levels were recovered in PIPKIβΔ456-expressing cells by coexpressing PIPKIβwt (Fig. 6 D). We detected a slight, nonsignificant reduction in phospho-MLC staining in cells expressing the kinase-dead $PIPKI\beta^{K138A}$ mutant (Fig. 6 D). As an antibody specificity control, *f*MLP-induced pS^{19}-MLC levels were reduced after cell treatment with the ROCK inhibitor Y27632 (Fig. S3 B).

The PIPKIβ C terminus interacts with EBP50, ERM proteins, and RhoGDI

We searched for proteins that interact with the 83aa-tail, using affinity purification of a dHL60 detergent extract on 83aa-tail GST fusion protein (Fig. 7 A). Four bands were selectively retained by the PIPKIβ 83aa-tail, which were identified by matrix-assisted laser desorption/ionization-time-of-flight (MALDI-TOF) mass spectrometry of tryptic digests as spectrin α, a 110-kD protein with spectrin β homology, moesin, and EBP50 (also termed sodium-proton exchanger regulatory factor 1), an adaptor for ERM proteins (Reczek et al., 1997). In addition, the 83aa-tail retained an unidentified ∼67-kD protein. Moesin represents more than 90% of the ERM proteins expressed in dHL60 cells (Ivetic and Ridley, 2004; and unpublished data); it is thus feasible that rescue of moesin in the pull-down assay indicates the ability of the 83aa-tail to interact with ERM proteins.

Immunofluorescence analysis of the proteins that bind the 83aa-tail indicated homogeneous spectrin α juxtamembrane staining in *f*MLP-stimulated dHL60 cells (unpublished data); in contrast, phospho-ERM and EBP50 polarized to the uropod of *f*MLP-stimulated PIPKIβwt-expressing cells (Fig. 7 B). Notably, PIPKIβΔ456 overexpression prevented polarization of these uropod markers (Fig. 7 C).

We tested 83aa-tail-GST binding to biotin-labeled, in vitro–translated moesin or EBP50. Recombinant moesin did not bind to 83aa-tail-GST (unpublished data), but in vitro–translated EBP50 bound very efficiently to the 83aa-tail-GST (Fig. 8 A); more important, the in vitro–translated moesin FERM (band 4.1 protein-ezrin-radixin-moesin) domain bound to the 83aa-tail-GST protein only in the presence of EBP50 (Fig. 8 A). These results suggested that EBP50 might regulate the interaction between ERM proteins and the PIPKIβ C terminus in a chemoattractant-dependent manner.

We analyzed the interaction of EBP50 and ERM proteins in PIPKIβwt- and PIPKIβΔ456-expressing cells. ERM proteins coprecipitated with PIPKIβwt after chemoattractant stimulation in immunoprecipitation assays; as predicted, this association was not observed for PIPKIβΔ456 (Fig. 8 B). Moreover, chemoattractant stimulation induced time-dependent association between ERM and EBP50, but only in cells overexpressing PIPKIβwt (Fig. 8 C); EBP50 appeared as a doublet in these immunoprecipitates, probably as a consequence of phosphorylation. Together, these results suggest that the PIPKIβ 83aa-tail regulates formation of a complex between ERM proteins and EBP50 after chemoattractant stimulation.

ERM proteins act upstream of Rho GTPases by interacting with RhoGDI, enabling RhoA activation (Takahashi et al., 1997). Based on the association between ERM proteins and the 83aa-tail, we found that chemoattractants induced coprecipitation of RhoGDI with overexpressed PIPKIβwt, whereas only a small amount PIPKIβΔ456 could be detected in these immunoprecipitates (Fig. 8, D and E). Moreover, we did not detect ERM-RhoGDI complexes in immunoprecipitates of PIPKIβΔ456-expressing cells (Fig. 8 E).

Discussion

Here we identified uropodal PIPKIβ localization as an important step in the organization of signaling involved in neutrophil polarity and chemotaxis. We found that (1) PIPKIβ polarized to the uropod after chemoattractant stimulation; (2) RNAi-induced knockdown of PIPKIβ impaired neutrophil polarity and chemotaxis as well as RhoA activation, indicating the relevance of the endogenous enzyme in these processes; (3) uropod PIPKIβ localization required the C-terminal 83aa-tail; (4) catalytically active or inactive PIPKIβ mutants lacking the C terminus prevented spatial and functional cell asymmetry and gradient sensing; and (5) the C-terminal 83aa-tail interacted with different adapters including, but not limited to, EBP50, moesin, and RhoGDI.

siRNA attenuation of PIPKIβ levels inhibited dHL60 cell polarity, impaired persistence during chemotaxis, and reduced chemoattractant-induced RhoA activation, although the effects were less dramatic than those observed for the PIPKIβΔ456 mutant. One explanation for these mild effects is that other PIPKI isozymes might compensate for the PIPKIβ deficiency. Results from PIPKIβ-null mice support this idea; although PIPKIβ has an exclusive role in modulating the actin cytoskeleton in mast cells, no major phenotypic defects were reported in these mice (Sasaki et al., 2005). The long $PIPKI\gamma^{661}$ isozyme is a candidate for PIPKIβ compensation, although a recent report suggests that this isoform is not required for G protein–coupled receptor-stimulated chemotaxis (Sun et al., 2007). The interplay between PIPKIβ and $PIPKI\gamma^{661}$ during leukocyte chemotaxis and the identity of their targets require further study.

Activation of ERM proteins requires two signals, $PI(4,5)P_2$ binding, and threonine phosphorylation within the actin-binding domain (Ivetic and Ridley, 2004). $PI(4,5)P_2$ is thought to recruit ERM proteins to the membrane by unfolding inactive monomers, whereas phosphorylation is believed to stabilize the active open conformation (Fievet et al., 2004). The FERM domain of active ERM proteins can then interact with RhoGDI, triggering RhoA activation (Takahashi et al., 1997); this in turn can induce further ERM activation through ROCK- or PIPKI-dependent mechanisms (Chong et al., 1994; Matsui et al., 1999; Santarius et al., 2006). In vitro kinase assays indicate that chemoattractants stimulate PIPKIβ-mediated $PI(4,5)P_2$ production.

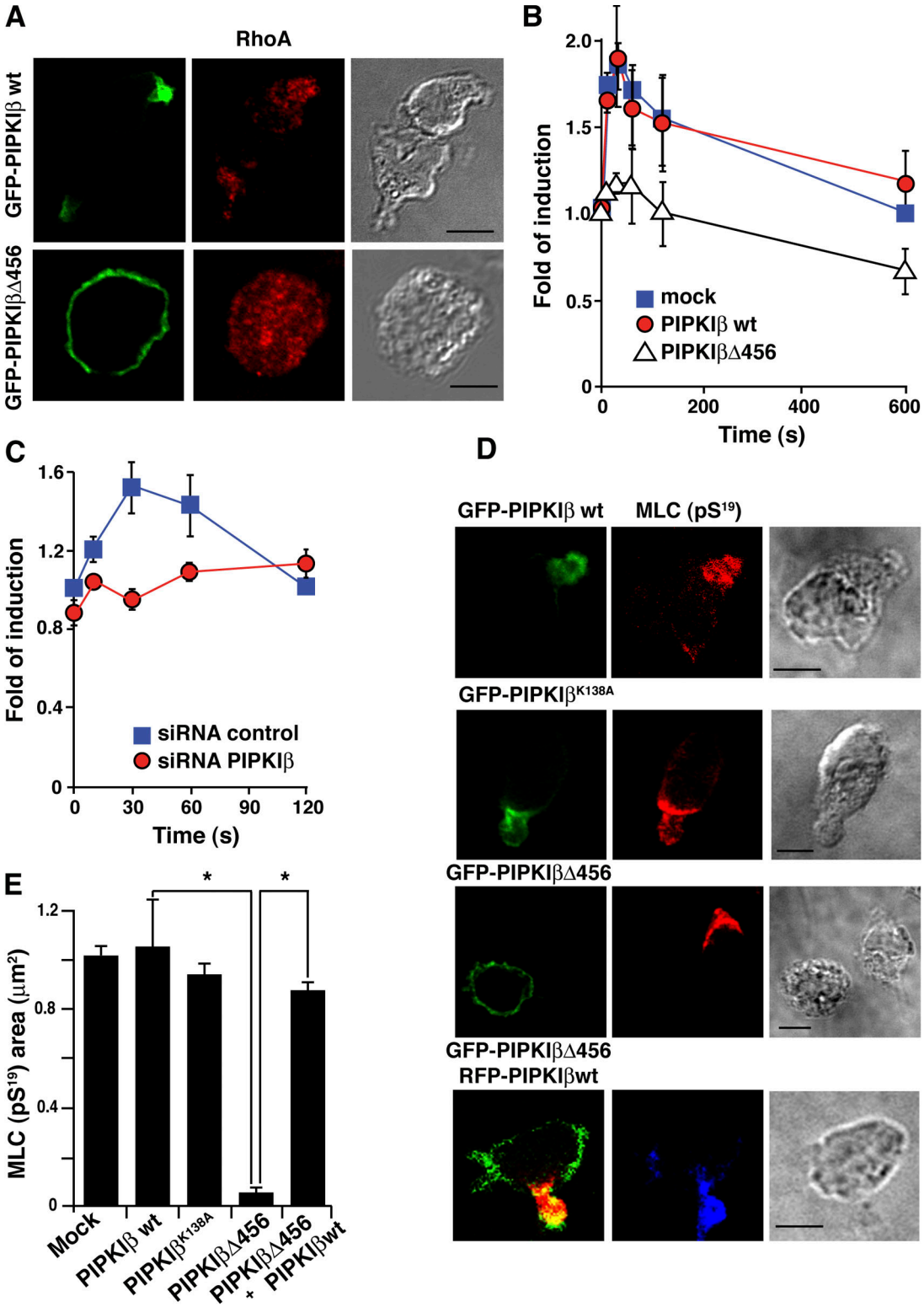

Figure 6. **PIPKIβ controls signaling at the uropod.** (A) PIPKIβwt- and PIPKIβΔ456-expressing dHL60 cells were exposed to uniform *f*MLP attractant, and stained with anti-RhoA antibody (red). Nomarski, red, and green channels are shown. Cells represent at least 15 cells ($n = 3$). (B) Mock-, PIPKIβwt- and PIPKIβΔ456-transfected HEK-293 cells were stimulated in suspension with CXCL12. At the times indicated, RhoA-GTP levels were determined with a luminometry-based assay. Values were normalized to those obtained in unstimulated cells and expressed as *x*-fold of induction. (C) Control or PIPKIβ-specific siRNA-transfected dHL60 cells were stimulated with *f*MLP and RhoA-GTP levels determined. Values were normalized to those obtained in unstimulated control siRNA-transfected cells. For B and C, data are mean ± SEM of values obtained in three independent experiments. (D) GFP-PIPKIβwt-, GFP-PIPKIβ^{K138A}-, and GFP-PIPKIβΔ456-expressing dHL60 cells, and cells coexpressing RFP-PIPKIβwt and GFP-PIPKIβΔ456 were stimulated as in A, and MLC phosphorylation analyzed by staining with a pS^{19}-MLC–specific antibody (red or blue, as indicated). (E) Quantification of the pS^{19}-MLC staining area of cells in D. Data are mean ± SEM of 20–35 cells recorded in three independent experiments. (*, $P < 0.05$, two-tailed Dunnett's test). Bar, 10 μm.

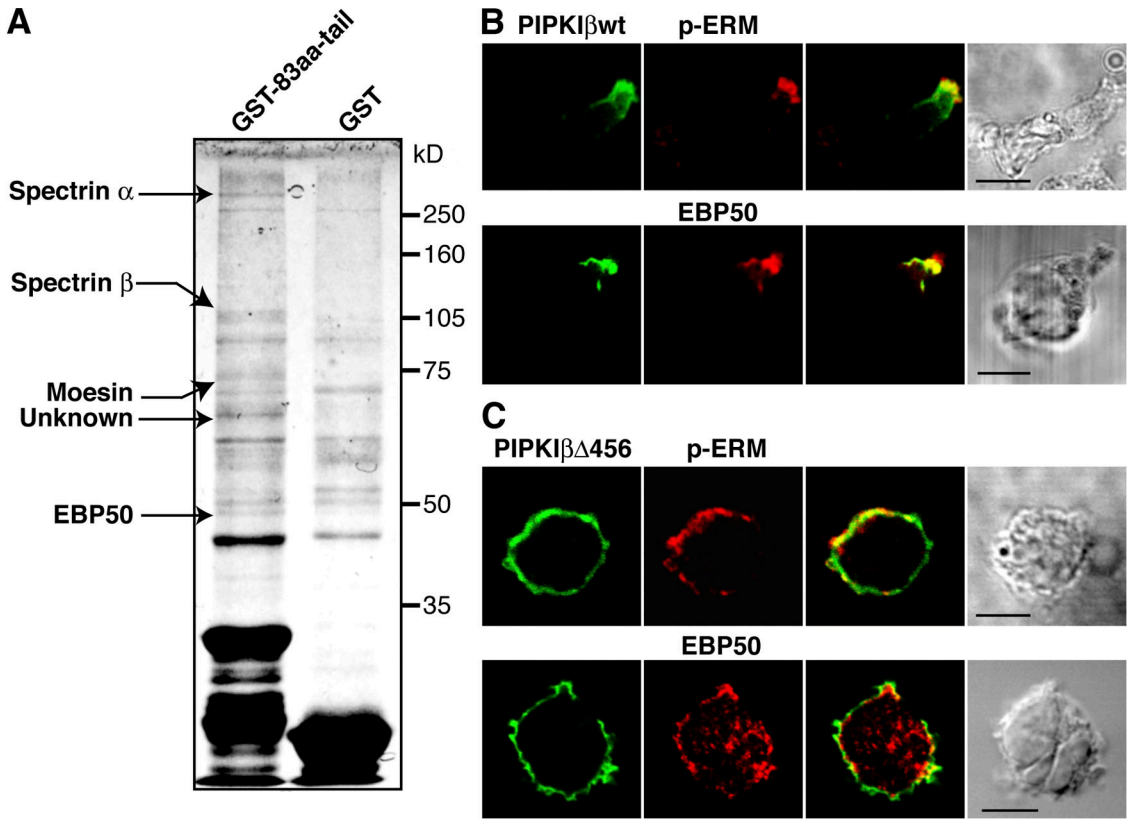

Figure 7. **The PIPKIβ C terminus interacts with moesin and EBP50.** (A) Pull-down assays were performed using the 83aa-tail fused to GST, or GST alone. Proteins were resolved in SDS-PAGE; proteins bound differentially to GST-83aa-tail and to GST were identified by MALDI-TOF mass spectrometry. Results shown are representative of two independent experiments. (B and C) Localization of endogenous phospho-ERM proteins (p-ERM) and EBP50 in GFP-PIPKIβwt- (B) and GFP-PIPKIβΔ456-expressing dHL60 cells (C) by immunofluorescence. Cells are representative of 30 cells recorded in two independent experiments; bar, 10 μm.

Local PIPKIβ-mediated $PI(4,5)P_2$ production might trigger ERM activation locally, initiating or boosting this feedback loop.

The phenotype observed in cells expressing the kinase-dead mutant is puzzling, however. Chemotaxing $PIPKI\beta^{K138A}$-expressing cells showed defects in tail retraction (Video 4) and a severe reduction in speed. Uropod detachment requires RhoA/ROCK-induced myosin II contraction (Alblas et al., 2001; Worthylake et al., 2001), suggesting that $PI(4,5)P_2$ production participates in PIPKIβ-mediated RhoA activation. Nonetheless, $PIPKI\beta^{K138A}$ expression only minimally affected pS^{19}-MLC phosphorylation, which is controlled by the RhoA/ROCK pathway. This result suggests that local PIPKIβ-induced $PI(4,5)P_2$ production is dispensable for RhoA activation; alternatively, PIPKIβ might regulate dHL60 cell chemotaxis via another mechanism(s) besides, or in addition to RhoA activation.

The most severe phenotype was observed in cells expressing the PIPKIβΔ456 mutant, which lacks the uropod targeting sequence in the 83aa-tail. PIPKIβΔ456-expressing cells cannot establish a stable front–rear asymmetry axis, leading to membrane ruffling or AKT-PH recruitment to cell edges up and down the gradient. PIPKIβΔ456 expression does not abrogate signals associated to the leading edge, but this mutant impaired chemoattractant-induced RhoA activation and pS^{19}-MLC phosphorylation in the uropod. Notably, ERM proteins did not coprecipitate detectably with RhoGDI in PIPKIβΔ456-overexpressing cells (Fig. 8). Based on these results, PIPKIβ polarization at the uropod might be a mechanism for signal localization at the cell posterior.

It is intriguing that these PIPKIβΔ456 effects occurred in cells expressing endogenous PIPKIβ, which suggests that PIPKIβΔ456 acts as a dominant-negative mutant. Chemoattractants stimulated PIPKIβΔ456-mediated $PI(4,5)P_2$ production; it is nonetheless unlikely that the PIPKIβΔ456 phenotype is a consequence of delocalized $PI(4,5)P_2$ synthesis because the kinase-dead $PIPKI\beta\Delta456^{K138A}$ mutant impedes cell polarity. PIPKIβΔ456 cannot engage the EBP50-ERM-RhoGDI complex (Fig. 8). The dominant-negative phenotype of the PIPKIβΔ456 mutant could be explained by assuming that the PIPKIβ N terminus or the common kinase domain might interact with other effectors or adaptors critical for neutrophil polarization. PIPKIβΔ456 would thus sequester these effectors/adaptors, preventing their interaction with endogenous PIPKIβ (which is expressed at much lower levels than the mutant). In support of this idea, co-expression of PIPKIβwt restored *f*MLP-induced polarization of PIPKIβΔ456-expressing dHL60 cells (Fig. 5 G). Identification of these additional PIPKIβ-interacting proteins will require future experiments.

In conclusion, we have determined that PIPKIβ is a new element in the regulation of neutrophil polarity and chemotaxis. PIPKIβ polarizes at the cell posterior through its C-terminal

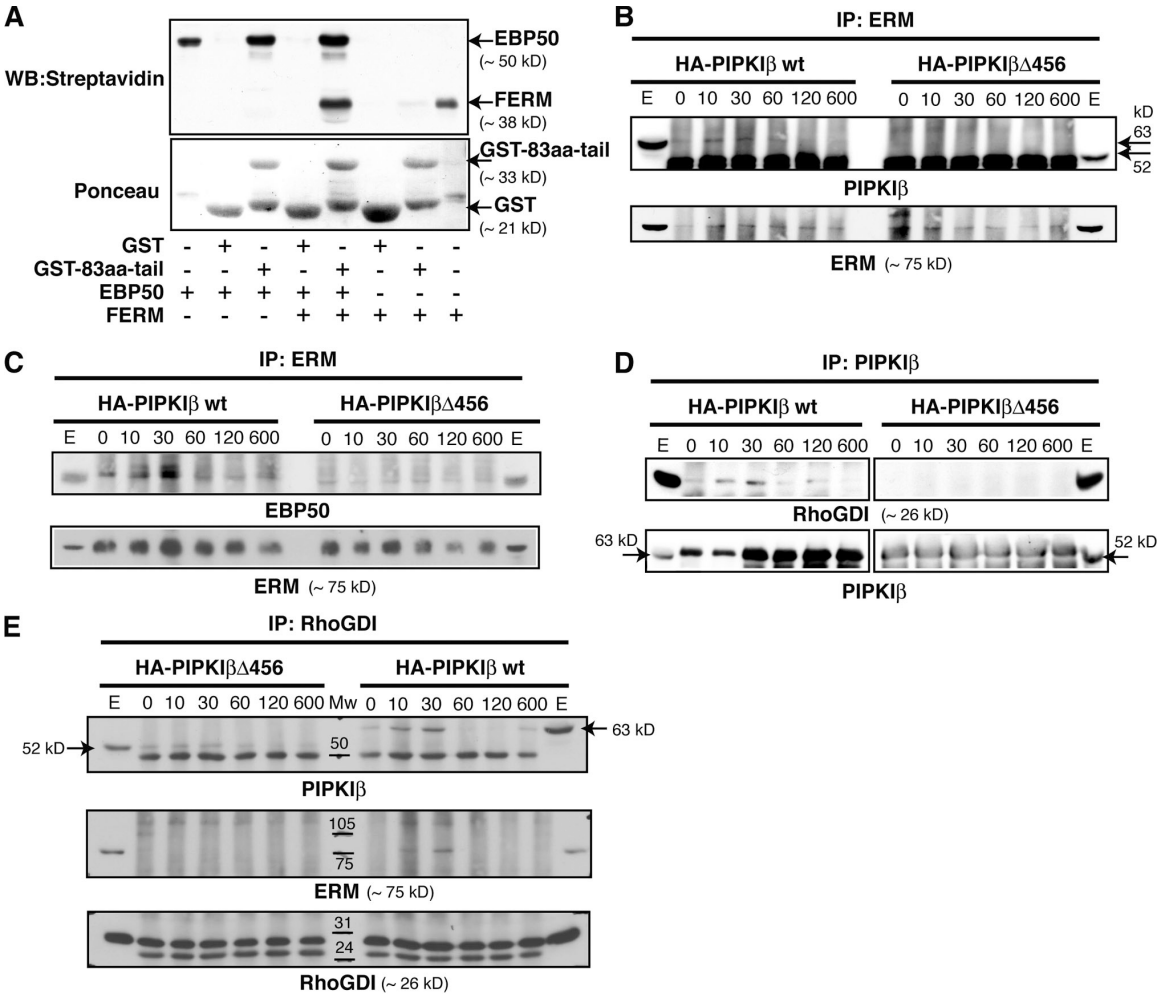

Figure 8. **The PIPKIβ C terminus regulates ERM protein interaction with RhoGDI.** (A) Equal amounts of GST-83aa-tail and GST proteins were incubated with 12 μl of biotinylated EBP50 and/or moesin FERM; bound proteins were analyzed by blotting with peroxidase-labeled streptavidin to detect biotinylated proteins (top panel) and Ponceau red for the GST and GST-83aa-tail (bottom panel). Relative migration of in vitro–translated EBP50 and moesin FERM domain (1 μl/lane) in the absence of GST proteins is shown (first and last lanes). (B) HA-tagged PIPKIβwt- and PIPKIβΔ456-expressing HEK-293 cells were stimulated in suspension with CXCL12 for the times indicated (in seconds). ERM proteins were immunoprecipitated and bound proteins analyzed sequentially with anti-HA and anti-ERM protein antibodies. Arrows indicate the relative migration of HA-PIPKIβwt- and HA-PIPKIβΔ456 proteins. E indicates cell extract. (C) The lysates in B were immunoprecipitated with anti-ERM protein antibody and blotted with anti-EBP50 and -ERM antibodies. (D) HEK-293 cells were cotransfected with myc-tagged RhoGDI and either HA-tagged PIPKIβwt or -PIPKIβΔ456, and stimulated in suspension with CXCL12. Cell lysates were immunoprecipitated with anti-HA antibodies and bound proteins blotted for RhoGDI (myc tag) and PIPKIβ (HA tag). (E) Cell lysates from CXCL12-stimulated HEK-293 cells coexpressing myc-RhoGDI and HA-PIPKIβwt- or HA-PIPKIβΔ456 were immunoprecipitated with anti-myc antibodies, then blotted sequentially with anti-HA, -ERM proteins, and -myc antibodies. Arrows indicate the relative migration of HA-PIPKIβwt and HA-PIPKIβΔ456. The blots are representative of three independent experiments.

domain, which interacts with other uropod proteins such as EBP50 and ERM. Given that EBP50 is a PDZ (postsynaptic density protein, disc-large, zonulin-1)-containing protein, it is possible that EBP50 links PIPKIβ to a network of PDZ proteins known to shape the uropod in other leukocytes (Ludford-Menting et al., 2005). PIPKIβ might thus participate in several signaling networks involved in leukocyte uropod identity.

Materials and methods

Antibodies and reagents

Anti–human PIPKIα, β, and γ, anti-myc clone 9E10, and anti-RhoA antibodies were obtained from Santa Cruz Biotechnology, Inc.; anti-phospho-ERM, -ERM, -pS^{19}-MLC, -phospho AKT, and -spectrin αII were from Cell Signaling Technology; anti-Rac and anti-AKT from Millipore; anti-EBP50 from Affinity BioReagents; anti-HA from Covance; anti-moesin from BD Biosciences; anti-ezrin from Invitrogen; peroxidase-labeled anti–mouse and anti–rabbit IgG from Dako; and biotinylated anti–rabbit IgG and cy2- and cy3-conjugated secondary antibodies from Jackson ImmunoResearch Laboratories. Anti-GST antibodies, Tri-reagent, PTX, Ficoll-Hypaque, Ponceau S red, fibronectin, DMSO, and *f*MLP were from Sigma-Aldrich; human CXCL12 was from PeproTech. The TNT transcription–translation system, Transcend Non-Radioactive Translation Detection Systems, trypsin, and peroxidase-labeled streptavidin were from Promega.

Cloning and generation of PIPKIβ mutants

cDNAs encoding mouse PIPKIα, β, and γ, and the kinase-dead PIPKIβ^{K138A} mutant were a gift of H. Isihara (University of Geneva, Geneva, Switzerland) and were subcloned in pEGFP-C1 (Clontech Laboratories, Inc.), pRFP-C3 (a gift of L. Rajendran, Max-Planck-Institute for Molecular Cell Biology and Genetics, Dresden, Germany), or pcDNA3.1-HA (a gift of T. Fischer; Centro Nacional de Biotecnología/CSIC, Madrid, Spain) to generate the GFP-, RFP-, and HA-chimeras, respectively. The deletion and

swapping mutants were generated using PCR and pfu Turbo DNA polymerase (Stratagene) and cloned in pEGFP-C1, pRFP-C3, and pcDNA3.1-HA (from T. Fischer; Centro Nacional de Biotecnología, Madrid, Spain) to obtain the corresponding tag-fusion proteins. The C-terminal fragment of PIPKIα (83aa-tail) was subcloned in pEGFP-C1 to generate the GFP chimera and in pGEX-4-T1 (GE Healthcare) for expression as a GST fusion protein in *Escherichia coli*. The ezrin FERM domain, a gift from M. Arpin (Institut Curie, Paris, France), was cloned in pcDNA3.1-HA and in pGEX-4-T1. The catalytically inactive $G\alpha_{12}^{(Q209L/D277N)}$ and $G\alpha_{13}^{(Q226L/D294N)}$ mutants (UMR cDNA Resource Center) were cloned in the pRV-IRES-GFP bicistronic plasmid (Genetrix). Dominant-negative $G\alpha_{12}$ and $G\alpha_{13}$ mutants were generated by cloning the C-terminal fragments of these G proteins in pCDNA3.1-HA. The Rac PBD was subcloned in pEGFP-C3; the GFP-PLCδ-PH domain was a gift of C. Schneider and P. Caroni (Friedrich Miescher Institute, Basel, Switzerland); myc-tagged RhoGDI was a gift of B. Olofsson (Centre National de la Recherche Scientifique, Gif-sur-Yvette, France). The EBP50 and moesin gene cDNA (Open Biosystems) were cloned in pCDNA3.1HA. The moesin FERM domain was amplified by PCR and cloned in pcDNA3.1-HA and in pGEX-4-T1. The GFP-AKT-PH domain and GFP-RhoN19 have been described (Gómez-Moutón et al., 2004).

Cell culture and transfections

HL60 cells were maintained in RPMI 1640 with 10% FCS and differentiated with 1.3% DMSO for 7 d. Differentiated cells were transfected with the indicated plasmids by electroporation (2×10^7 cells, 320 mV, 1,000 μF) in an electroporator (Bio-Rad Laboratories), or using the T Cell Nucleofector kit (Amaxa Biosystems); protein expression was analyzed 6–12 h after transfection by FACS (Beckman Coulter), and live cells isolated on Ficoll-Hypaque gradients. Transfection efficiency was typically 15–20%. Jurkat cells were cultured in RPMI 1640 with 10% FCS and transfected as described (Gómez-Moutón et al., 2004). HEK-293 cells were maintained in DME with 10% FCS. Cells were transiently transfected with the indicated plasmids using the standard calcium phosphate method, and protein expression analyzed 48 h later (transfection efficiency was 70–80%).

siRNA experiments

dHL60 cells were transfected with two human PIPKIβ-specific or nonspecific siRNA duplexes (50 nM; Dharmacon) using Jet-siENDO (Polyplus Transfection). The sequences of the PIPKIβ-specific siRNA duplexes were: 5′-GGCAGACAGAUUUCUUAAGUUU-3′ and 5′-UAAGACAUACGUCCAUUAUU-3′. In all experiments, a Cy3-labeled nonspecific duplex control (Dharmacon) was transfected with control or specific duplexes to determine transfection efficiency (usually 98–100% by FACS). PIPKIβ silencing was analyzed 24 and 48 h after transfection by quantitative RT-PCR using Taqman probes (Applied Biosystems) specific for the human PIPKα, β, and γ genes. ΔCt values provided by the software of the apparatus were normalized using 18S RNA, and the relative mRNA levels calculated using the formula $2 - (\Delta Ct \text{ sample} - \Delta Ct \text{ control})$. GAPDH amplification was performed in each experiment as an internal control. PIPKIβ silencing was analyzed 48 h after transfection by sequential immunoblotting with anti-PIPKIβ and anti-actin (loading control) antibodies.

Time-lapse confocal videomicroscopy and chemotaxis assays

Real-time cell chemotaxis was studied by time-lapse confocal microscopy as described (Gómez-Moutón et al., 2004). Starved cells were plated (1 h, 37°C) on fibronectin-coated chamber coverslips (Nunc) and stimulated with *f*MLP (100 nM) applied with a micropipette at 37°C. Fluorescence and phase-contrast images were recorded in a confocal microscope (TCS-NT; Leica) with a 63× NA1.4 oil plan-Apo objective with an electronic zoom of 2 at established time intervals. Brightness and/or contrast were adjusted, and videos were processed with ImageJ software (National Institutes of Health, Bethesda, MD). Motility parameters and cell tracks from these videos were obtained using the MetaMorph Imaging System (Meta Imaging Software). The directional index was calculated as the net distance moved toward the chemoattractant source divided by the cumulative length of the migration path. Cell velocity was defined as the net distance divided by the time used to cover it. Plots showing trajectories of different cells were composed in Adobe Photoshop.

For transwell assays, $1–2 \times 10^5$ PIPKIβ-expressing, Y-27632-pretreated (10 μM, 1 h; Calbiochem), or siRNA-transfected dHL60 cells were seeded in the upper chamber in serum-free medium; lower chambers were filled with serum-free medium alone or containing *f*MLP (100 nM). Transmigrated cells were quantified by FACS after incubation (2.5 h, 37°C). The percentage of migrating cells was calculated as the quotient of the number of migrating fluorescent cells in the lower chamber and the fluorescent cells in the initial input.

Immunofluorescence and cell polarity assays

Serum-starved Jurkat- and dHL60-transfected cells were plated on fibronectin-coated slides and, after incubation (1 h, 37°C), were stimulated with CXCL12 (100 nM, 10 min, 37°C) or *f*MLP (100 nM, 3 min, 37°C). After washing, plates were fixed with 3.7% paraformaldehyde (10 min, 20°C) in PBS, permeabilized with 0.1% Triton X-100 (5 min, 20°C), and incubated (1 h, 4°C) with the indicated primary antibody, followed by the appropriate Cy2- or Cy3-conjugated secondary antibody. Samples were mounted in Vectashield medium (Vector Laboratories) and images recorded in a confocal microscope (Fluoview 10; Olympus) with a 60× 1.4NA oil plan-Apo objective, using FV10-ASW 1.6 software (Olympus). Brightness and/or contrast were adjusted with ImageJ software. In some experiments, starved cells were treated with PTX (0.5 mg/ml, 16 h, 37°C) or Y-27632 (10 μM, 1 h, 37°C), and plated on Fn-coated slides. PTX and Y-27632 were maintained throughout the assay.

Cell polarization in siRNA-transfected cells was determined by F-actin staining with phalloidin-rhodamine (Invitrogen) and anti-phospho-ERM. Cells showing both accumulation of actin at the leading edge and phospho-ERM at the uropod were scored as polarized. Eight random fields were recorded per condition and at least 200 cells were counted per sample in three independent experiments.

$pSer^{19}$-MLC levels were quantified as described (Jiménez-Baranda et al., 2007). In brief, dHL-60 cells stained with anti-$pSer^{19}$-MLC antibody and were serially scanned in horizontal sections 0.6 μm apart; section 4 was used for quantification. The same black and white threshold was then applied to all images collected (upper threshold level 76, lower threshold level 30). The image was scaled (512 pixels = 152.4 μm; pixel/aspect ratio = 1) and particle measurement automatically performed using ImageJ software.

Lipid kinase assays

Serum-starved mock-, HA-PIPKIβ-, HA-$PIPKI\beta^{K138A}$-, HA-PIPKIβΔ456-, and HA-$PIPKI\beta\Delta456^{K138A}$-expressing HEK-293 cells were stimulated in suspension with CXCL12 (100 nM, 1 min, 37°C) for the times indicated. HA-tagged enzymes were immunoprecipitated from cell extracts and lipid kinase activity was determined as described (Jones et al., 2000). The kinase reaction mix (50 μl) contained 200 μM PI4P (Echelon Biosciences), 20 μM ATP, 10 mM $MgCl_2$, and 10 μCi [γ^{32}]ATP (GE Healthcare). Radioactive spots with an R*f* value corresponding to PI(4,5)P_2 were identified by autoradiography after TLC.

The amount of PI(4,5)P_2 was measured in cell extracts from mock-, PIPKIβ-, and PIPKIβΔ456-expressing HEK-293 cells before and after CXCL12 stimulation (100 nM, 2 min, 37°C) using the PI(4,5)P_2 Mass Strip kit (Echelon Biosciences) according to the supplier's protocol.

Rho activation assay

RhoA activity was determined using the luminescence-based G-LISA RhoA Activation Assay Biochem kit (Cytoskeleton, Inc.). PIPKIβ-specific and mismatched siRNA transfected-dHL60 cells or mock-, PIPKIβ-, or PIPKIβΔ456-expressing HEK-293 cells were starved and maintained in suspension. Cells were stimulated with *f*MLP (100 nM) or CXCL12 (100 nM) for the indicated times and assayed according to the supplier's protocol.

In vitro and in vivo analysis of PIPKIβ interactions

For pull-down assays, GST-83aa-tail or GST proteins were produced in *E. coli* and purified using glutathione Sepharose 4B (GE Healthcare). dHL60 cells (2×10^8) were stimulated with *f*MLP (100 nM, 5 min, 37°C) and extracts were prepared immediately with RIPA buffer (50 mM Tris-HCl, pH 7.5, 0.15 M NaCl, 0.1% SDS, 0.5% deoxycholate, and 1% NP-40). After preclearing with GST, cell extracts were incubated (overnight, 4°C) with GST-83aa-tail or GST bound to glutathione Sepharose. Beads were washed and retained proteins eluted with SDS sample buffer; after boiling for 5 min, proteins were resolved by SDS-PAGE and stained with Coomassie blue. Protein identification was performed by the Proteomics Core Facility (see below).

Pull-down assays were also performed with in vitro–transcribed and –translated EBP50, moesin, and HA-moesin FERM domain using the TNT system (T7 promoter), incorporating biotinylated lysine residues in the nascent proteins. Interaction of the GST-83aa-tail or GST with the prey proteins was performed in binding buffer (PBS, 1% BSA, 0.02% Triton X-100) for 1 h at 4°C. After washing with PBS containing 0.05% Triton X-100, the proteins were eluted in SDS sample buffer and analyzed by immunoblot using peroxidase-labeled streptavidin. Before immunoblotting, nitrocellulose membranes were stained with Ponceau S red to visualize GST proteins.

For immunoprecipitation, serum-starved HEK-293 cells transfected with PIPKIβ or PIPKIβΔ456 were stimulated in suspension with 100 nM CXCL12 (37°C) for the indicated times, placed on ice, washed with ice-cold PBS, and lysed with RIPA buffer. Cell extracts (300 μg) were immunoprecipitated (2 h, 4°C) with anti-HA, -ERM, -myc, or –mouse IgG antibody, followed by incubation (1 h, 4°C) with Gamma-Bind Plus Sepharose (GE Healthcare). Immunoprecipitates were resolved in SDS-PAGE and analyzed by immunoblot with anti-HA, -ERM, and -myc antibodies.

Proteomic techniques

Proteins from stained one-dimensional polyacrylamide gels were excised and processed in 96-well plates in a Proteineer DP (Bruker Daltonics). For protein digestion, gel plugs were washed with 50 mM NH_4HCO_3 and treated with acetonitrile before reduction (10 mM DTT in 25 mM NH_4HCO_3) and alkylation (55 mM iodoacetamide in 50 mM NH_4HCO_3). Proteins were trypsin-digested (15 ng/μl in 25 mM NH_4HCO_3, 4 h, 37°C). Peptides were eluted from gel pieces with 0.5% trifluoroacetic acid (TFA) in water (30 min, 25°C). Peptides were analyzed by MALDI-TOF MS; 0.5 μl matrix solution (5 mg/ml 2,5-dihydrobenzoic acid in 33% [vol/vol] aqueous acetonitrile and 0.1% [vol/vol] TFA) was added to a 600-μm Anchor-Chip MALDI target (Bruker Daltonics) and dried at room temperature. A 0.5 μl aliquot of each peptide mixture was deposited onto matrix spots and dried.

MALDI peptide mass fingerprinting was acquired on a Bruker Reflex IV MALDI-TOF mass spectrometer with SCOUT source in positive ion reflector mode (ion acceleration voltage 23 kV). Spectra were acquired with FlexControl 2.4 and processed with Flex Analysis 2.4. Equipment was externally calibrated using protonated mass signals from a peptide mixture (1,000–3,500 m/z range). For peak list generation, each spectrum was internally calibrated with two known trypsin autoproteolysis peptides; typical mass measurement accuracy was ±30 ppm (800–3,000 m/z range). Data analysis parameters were a signal-to-noise threshold of 20 and resolution >4,000.

For protein identification, the tryptic peptide masses were batch processed and searched against the nonredundant National Center for Biotechnology Information (NCBI) database using Mascot 2.1 (Matrix Science) through the Bruker Biotools 2.0 interface. Search parameters were carbamidomethyl cysteine (fixed modification), oxidized methionines (variable modification), peptide mass tolerance of 80 ppm, with one missed cleavage site allowed. For all proteins, the probability-based Mowse scores were greater than the minimum score fixed as significant ($P < 0.02$).

Statistical analysis

Data are expressed as mean ± SEM. Dunnett two-tailed or Student's two-tailed *t* tests were used to compare differences between groups in various experiments.

Online supplemental material

Figure S1 shows the analysis of HA-tagged PIPKIβ localization in dHL60 neutrophil-like cells and Jurkat T cells, as well as additional images for endogenous PIPKI isoforms and the kinase-dead PIPKIβ^{K138A} mutant in *f*MLP-stimulated cells. Figure S2 shows the analysis of PI(4,5)P_2 and PIP_3 levels in PIPKIβ-expressing cells. Figure S3 shows the analysis of RhoA activity in dHL60 and HEK-293 cells stimulated with *f*MLP and CXCL12, respectively, as well as analysis of antibody specificity for pS^{19}-MLC. Video 1 shows PIPKIβ polarization to the uropod during dHL60 cell chemotaxis. Video 2 shows that PIPKIα does not polarize during dHL60 cell chemotaxis. Video 3 shows the homogeneous distribution of PIPKIγ^{635} during dHL60 cell chemotaxis. Video 4 shows distribution of the kinase-dead PIPKIβ^{K138A} mutant during dHL60 cell chemotaxis. Video 5 shows the cellular localization of the C terminus–deleted PIPKIγ$^{1–502}$ mutant in chemotaxing dHL60 cells. Video 6 shows the dynamics of the GFP-tagged chimera formed by the C terminus–deleted PIPKIγ$^{1–502}$ mutant and the PIPKIβ C terminus (PIPKIγ$^{1–502}$β$^{455–539}$), during chemotaxis toward *f*MLP. Video 7 shows time-lapse confocal images of dHL60 cells coexpressing AKT-PH-GFP and RFP-PIPKIβwt migrating toward *f*MLP. Video 8 shows that overexpression of the PIPKIβΔ456 mutant impedes polarization of PI3K signaling in directionally stimulated dHL60 cells. Video 9 shows that PIPKIβwt-expressing dHL60 cells persistently polarize Rac signaling during chemotaxis. Video 10 shows that PIPKIβΔ456 overexpression inhibits polarization of Rac signaling in directionally stimulated dHL60 cells. Online supplemental material is available at http://www.jcb.org/cgi/content/full/jcb.200705044/DC1.

We are grateful to H. Isihara, M. Arpin, C. Schneider, P. Caroni, B. Olofsson, L. Rajendran, and T. Fischer for reagents and helpful comments. We thank E. Mira, C. Gómez-Moutón, and S. Jiménez-Baranda for critical reading of the manuscript; A. Zaballos and L. Almonacid for quantitative PCR analysis; C. Sánchez and A. Muñoz for help with MetaMorph software; S. Juárez for help in proteomic analysis; and C. Mark for editorial assistance.

This work was supported in part by the Spanish Ministry of Education and Science (SAF2005-00241 and NAN2004-08805-C04/04 to S. Mañes, and BFU2004-01756 to I. Mérida), and the European Union FP6 (INNOCHEM, FP6 LSHB-CT-2005-518167) to S. Mañes and C. Martínez-A. The Department of Immunology and Oncology was founded and is supported by the Spanish National Research Council (CSIC) and by Pfizer.

Submitted: 8 May 2007
Accepted: 24 November 2007

References

Alblas, J., L. Ulfman, P. Hordijk, and L. Koenderman. 2001. Activation of RhoA and ROCK are essential for detachment of migrating leukocytes. *Mol. Biol. Cell.* 12:2137–2145.

Arioka, M., S. Nakashima, Y. Shibasaki, and K. Kitamoto. 2004. Dibasic amino acid residues at the carboxy-terminal end of kinase homology domain participate in the plasma membrane localization and function of phosphatidylinositol 5-kinase γ. *Biochem. Biophys. Res. Commun.* 319:456–463.

Campello, S., R.A. Lacalle, M. Bettella, S. Mañes, L. Scorrano, and A. Viola. 2006. Orchestration of lymphocyte chemotaxis by mitochondrial dynamics. *J. Exp. Med.* 203:2879–2886.

Caroni, P. 2001. New EMBO members' review: actin cytoskeleton regulation through modulation of PI(4,5)P(2) rafts. *EMBO J.* 20:4332–4336.

Charest, P.G., and R.A. Firtel. 2006. Feedback signaling controls leading-edge formation during chemotaxis. *Curr. Opin. Genet. Dev.* 16:339–347.

Chong, L.D., A. Traynor-Kaplan, G.M. Bokoch, and M.A. Schwartz. 1994. The small GTP-binding protein Rho regulates a phosphatidylinositol 4-phosphate 5-kinase in mammalian cells. *Cell.* 79:507–513.

Cronshaw, D.G., A. Kouroumalis, R. Parry, A. Webb, Z. Brown, and S.G. Ward. 2006. Evidence that phospholipase-C-dependent, calcium-independent mechanisms are required for directional migration of T-lymphocytes in response to the CCR4 ligands CCL17 and CCL22. *J. Leukoc. Biol.* 79:1369–1380.

Fievet, B., A. Gautreau, C. Roy, L. Del Maestro, P. Mangeat, D. Louvard, and M. Arpin. 2004. Phosphoinositide binding and phosphorylation act sequentially in the activation mechanism of ezrin. *J. Cell Biol.* 164:653–659.

Filippi, M.D., K. Szczur, C.E. Harris, and P.Y. Berclaz. 2007. Rho GTPase Rac1 is critical for neutrophil migration into the lung. *Blood.* 109:1257–1264.

Gardiner, E.M., K.N. Pestonjamasp, B.P. Bohl, C. Chamberlain, K.M. Hahn, and G.M. Bokoch. 2002. Spatial and temporal analysis of Rac activation during live neutrophil chemotaxis. *Curr. Biol.* 12:2029–2034.

Gómez-Moutón, C., J. Abad, E. Mira, R. Lacalle, E. Gallardo, S. Jiménez-Baranda, I. Illa, A. Bernad, S. Mañes, and C. Martínez-A. 2001. Segregation of leading-edge and uropod components into specific lipid rafts during T cell polarization. *Proc. Natl. Acad. Sci. USA.* 98:9642–9647.

Gómez-Moutón, C., R.A. Lacalle, E. Mira, S. Jiménez-Baranda, D.F. Barber, A.C. Carrera, C. Martínez-A., and S. Mañes. 2004. Dynamic redistribution of raft domains as an organizing platform for signaling during cell chemotaxis. *J. Cell Biol.* 164:759–768.

Ishihara, H., Y. Shibasaki, N. Kizuki, T. Wada, Y. Yazaki, T. Asano, and Y. Oka. 1998. Type I phosphatidylinositol-4-phosphate 5-kinases. Cloning of the third isoform and deletion/substitution analysis of members of this novel lipid kinase family. *J. Biol. Chem.* 273:8741–8748.

Itoh, T., H. Ishihara, Y. Shibasaki, Y. Oka, and T. Takenawa. 2000. Autophosphorylation of type I phosphatidylinositol phosphate kinase regulates its lipid kinase activity. *J. Biol. Chem.* 275:19389–19394.

Ivetic, A., and A. Ridley. 2004. Ezrin/radixin/moesin proteins and Rho GTPase signalling in leucocytes. *Immunology.* 112:165–176.

Jiménez-Baranda, S., C. Gómez-Moutón, A. Rojas, L. Martínez-Prats, E. Mira, R.A. Lacalle, A. Valencia, D.S. Dimitrov, A. Viola, R. Delgado, et al. 2007. Filamin-A regulates actin-dependent clustering of HIV receptors. *Nat. Cell Biol.* 9:838–846.

Jones, D.R., M.A. Sanjuan, and I. Merida. 2000. Type Ialpha phosphatidylinositol 4-phosphate 5-kinase is a putative target for increased intracellular phosphatidic acid. *FEBS Lett.* 476:160–165.

Kimura, K., M. Ito, M. Amano, K. Chihara, Y. Fukata, M. Nakafuku, B. Yamamori, J. Feng, T. Nakano, K. Okawa, et al. 1996. Regulation of myosin phosphatase by Rho and Rho-associated kinase (Rho-kinase). *Science.* 273:245–248.

Lacalle, R.A., C. Gómez-Moutón, D.F. Barber, S. Jiménez-Baranda, E. Mira, C. Martínez-A., A.C. Carrera, and S. Mañes. 2004. PTEN regulates

motility but not directionality during leukocyte chemotaxis. *J. Cell Sci.* 117:6207–6215.

Lee, J., T. Katakai, T. Hara, H. Gonda, M. Sugai, and A. Shimizu. 2004. Roles of p-ERM and Rho-ROCK signaling in lymphocyte polarity and uropod formation. *J. Cell Biol.* 167:327–337.

Li, Z., X. Dong, Z. Wang, W. Liu, N. Deng, Y. Ding, L. Tang, T. Hla, R. Zeng, L. Li, and D. Wu. 2005. Regulation of PTEN by Rho small GTPases. *Nat. Cell Biol.* 7:399–404.

Ling, K., N. Schill, M. Wagoner, Y. Sun, and R.A. Anderson. 2006. Movin' on up: the role of PtdIns(4,5)P(2) in cell migration. *Trends Cell Biol.* 16:276–284.

Ludford-Menting, M.J., J. Oliaro, F. Sacirbegovic, E.T. Cheah, N. Pedersen, S.J. Thomas, A. Pasam, R. Iazzolino, L.E. Dow, N.J. Waterhouse, et al. 2005. A network of PDZ-containing proteins regulates T cell polarity and morphology during migration and immunological synapse formation. *Immunity.* 22:737–748.

Matsui, T., S. Yonemura, S. Tsukita, and S. Tsukita. 1999. Activation of ERM proteins in vivo by Rho involves phosphatidyl-inositol 4-phosphate 5-kinase and not ROCK kinases. *Curr. Biol.* 9:1259–1262.

Mañes, S., and A. Viola. 2006. Lipid rafts in lymphocyte activation and migration. *Mol. Membr. Biol.* 23:59–69.

Mañes, S., C. Gómez-Moutón, R. Lacalle, S. Jiménez-Baranda, E. Mira, and C. Martínez-A. 2005. Mastering time and space: immune cell polarization and chemotaxis. *Semin. Immunol.* 17:77–86.

Mouneimne, G., V. DesMarais, M. Sidani, E. Scemes, W. Wang, X. Song, R. Eddy, and J. Condeelis. 2006. Spatial and temporal control of cofilin activity is required for directional sensing during chemotaxis. *Curr. Biol.* 16:2193–2205.

Nishio, M., K. Watanabe, J. Sasaki, C. Taya, S. Takasuga, R. Iizuka, T. Balla, M. Yamazaki, H. Watanabe, R. Itoh, et al. 2007. Control of cell polarity and motility by the PtdIns(3,4,5)P3 phosphatase SHIP1. *Nat. Cell Biol.* 9:36–44.

Nombela-Arrieta, C., R.A. Lacalle, M.C. Montoya, Y. Kunisaki, D. Megias, M. Marques, A.C. Carrera, S. Mañes, Y. Fukui, A.C. Martinez, and J.V. Stein. 2004. Differential requirements for DOCK2 and phosphoinositide-3-kinase gamma during T and B lymphocyte homing. *Immunity.* 21:429–441.

Nuzzi, P.A., M.A. Senetar, and A. Huttenlocher. 2007. Asymmetric localization of calpain 2 during neutrophil chemotaxis. *Mol. Biol. Cell.* 18:795–805.

Rameh, L., K. Tolias, B. Duckworth, and L. Cantley. 1997. A new pathway for synthesis of phosphatidylinositol-4,5-bis-phosphate. *Nature.* 390:192–196.

Rebecchi, M., and S. Pentyala. 2000. Structure, function, and control of phosphoinositide-specific phospholipase C. *Physiol. Rev.* 80:1291–1335.

Reczek, D., M. Berryman, and A. Bretscher. 1997. Identification of EBP50: A PDZ-containing phosphoprotein that associates with members of the ezrin-radixin-moesin family. *J. Cell Biol.* 139:169–179.

Ridley, A., M. Schwartz, K. Burridge, R. Firtel, M. Ginsberg, G. Borisy, J. Parsons, and A. Horwitz. 2003. Cell Migration: Integrating signals from front to back. *Science.* 302:1704–1709.

Santarius, M., C.H. Lee, and R.A. Anderson. 2006. Supervised membrane swimming: small G-protein lifeguards regulate PIPK signalling and monitor intracellular PtdIns(4,5)P2 pools. *Biochem. J.* 398:1–13.

Sasaki, J., T. Sasaki, M. Yamazaki, K. Matsuoka, C. Taya, H. Shitara, S. Takasuga, M. Nishio, K. Mizuno, T. Wada, et al. 2005. Regulation of anaphylactic responses by phosphatidylinositol phosphate kinase type Iα. *J. Exp. Med.* 201:859–870.

Sun, Y., K. Ling, M.P. Wagoner, and R.A. Anderson. 2007. Type I gamma phosphatidylinositol phosphate kinase is required for EGF-stimulated directional cell migration. *J. Cell Biol.* 178:297–308.

Takahashi, K., T. Sasaki, A. Mammoto, K. Takaishi, T. Kameyama, S. Tsukita, and Y. Takai. 1997. Direct interaction of the Rho GDP dissociation inhibitor with ezrin/radixin/moesin initiates the activation of the Rho small G protein. *J. Biol. Chem.* 272:23371–23375.

Tan, W., D. Martin, and J.S. Gutkind. 2006. The Galpha13-Rho signaling axis is required for SDF-1-induced migration through CXCR4. *J. Biol. Chem.* 281:39542–39549.

Van Keymeulen, A., K. Wong, Z. Knight, C. Govaerts, K. Hahn, K. Shokat, and H. Bourne. 2006. To stabilize neutrophil polarity, PIP3 and Cdc42 augment RhoA activity at the back as well as signals at the front. *J. Cell Biol.* 174:437–445.

Willard, S.S., and P.N. Devreotes. 2006. Signaling pathways mediating chemotaxis in the social amoeba, Dictyostelium discoideum. *Eur. J. Cell Biol.* 85:897–904.

Worthylake, R.A., S. Lemoine, J.M. Watson, and K. Burridge. 2001. RhoA is required for monocyte tail retraction during transendothelial migration. *J. Cell Biol.* 154:147–160.

Xu, J., F. Wang, A. Van Keymeulen, P. Herzmark, A. Straight, K. Kelly, Y. Takuwa, N. Sugimoto, T. Mitchison, and H. Bourne. 2003. Divergent signals and cytoskeletal assemblies regulate self-organizing polarity in neutrophils. *Cell.* 114:201–214.

Yonemura, S., T. Matsui, S. Tsukita, and S. Tsukita. 2002. Rho-dependent and -independent activation mechanisms of ezrin/radixin/moesin proteins: an essential role for polyphosphoinositides *in vivo*. *J. Cell Sci.* 115:2569–2580.

Yoshinaga-Ohara, N., A. Takahashi, T. Uchiyama, and M. Sasada. 2002. Spatiotemporal regulation of moesin phosphorylation and rear release by Rho and serine/threonine phosphatase during neutrophil migration. *Exp. Cell Res.* 278:112–122.